CHALMERS

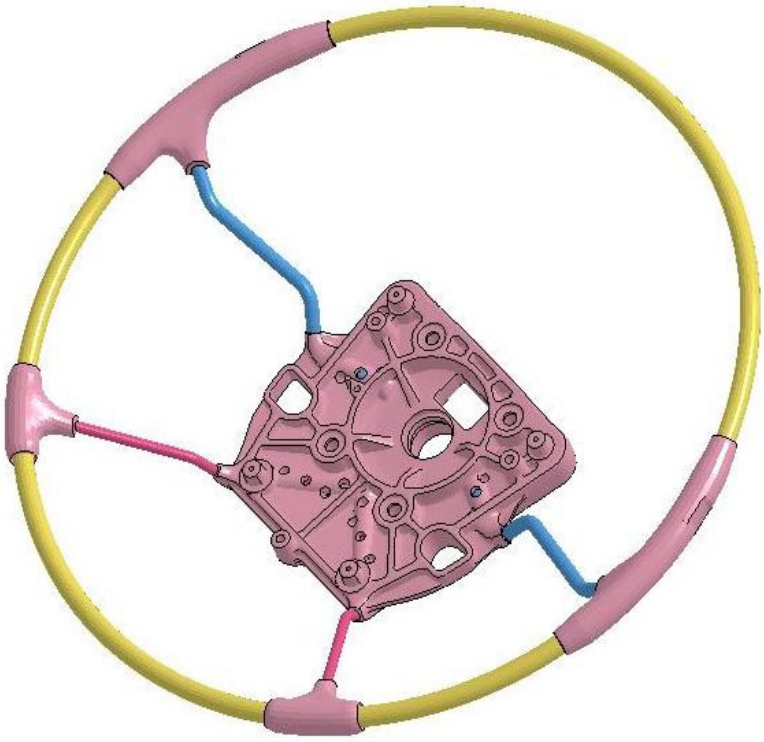

Finite Element Steering Wheel for Heavy Vehicles, Testing and Modeling.

Master's Thesis in the Automotive Engineering

ANEES UR REHMAN

MEHDI ESMAEILI NAJAFABADI

Department of Applied Mechanics
Division of Vehicle Safety
CHALMERS UNIVERSITY OF TECHNOLOGY
Göteborg, Sweden 2011
Master's Thesis 2011:66

MASTER'S THESIS 2011:66

Finite Element Steering Wheel for Heavy Vehicles, Testing and Modeling.

Master's Thesis in Automotive Engineering

ANEES UR REHMAN

MEHDI ESMAEILI NAJAFABADI

Department of Applied Mechanics
Division of Vehicle Safety
CHALMERS UNIVERSITY OF TECHNOLOGY
Göteborg, Sweden 2011

Finite Element Steering Wheel for Heavy Vehicles, Testing and Modeling

Master's Thesis in the Master's program Automotive Engineering

ANEES UR REHMAN

MEHDI ESMAEILI NAJAFABADI

Master's Thesis 2011:66
ISSN 1652-8557
Department of Applied Mechanics
Division of Vehicle Safety
Chalmers University of Technology
SE-412 96 Göteborg
Sweden
Telephone: + 46 (0)31-772 1000

Chalmers Reproservice
Göteborg, Sweden 2011

Finite Element Steering Wheel for Heavy Vehicles, Testing and Modeling Master's Thesis in Automotive Engineering

ANEES UR REHMAN & MEHDI ESMAEILI NAJAFABADI

Division of Vehicle Safety
Department of Applied Mechanics
Chalmers University of Technology

ABSTRACT

The main aim of this study was to validate an already existing Finite Element (FE) model of a truck steering wheel, using experimental testing and computer modeling.

Statistics show a high risk of sustaining severe injuries, in a frontal crash of heavy vehicles, due to steering wheel rim to thorax contact. The Hybrid III crash test dummy is now also used for analyzing heavy vehicle frontal crashes. It was originally developed for passenger cars and load cases common to them. To use in heavy vehicles, loading pattern to Hybrid III torso is now changed from the central hub to the rim of steering wheel. The Hybrid III crash test dummy is also available in FE codes. In order to investigate the heavy vehicle crashes in FE, a validated FE steering wheel model is also required.

An impact test setup was designed and replicated both in physical testing and computer modeling. Since the steering wheel can be adjusted at different tilt angles of the rim during driving, a set of tilt angles 0, 10, 20 and 30 degree was selected to see the behavior of steering wheel on impact with the rigid steel plate. The contact force, impact plate displacement and component deformations were the key parameters to be observed and compared, in order to validate the FE steering wheel model.

During physical tests for all the tilt angles, the steering wheel showed a stiff behavior regarding force level and horizontal displacement of the impact plate. Variation in peak force level during simulation and physical tests is less than 5% for 0 and 10 degree. The simulation results were considered validated for 78 mm and 66 mm of impact plate displacement for 0 and 10 degree respectively. Similarly, peak force level was found 26% and 45% higher in physical tests for 20 and 30 degree respectively. The simulation results were found out of the corridor limits, and FE model was not considered as validated for 20 and 30 degree tilt angles.

Presence of foam is found one of the major differences between the steering wheel and its FE model, as this foam absorbs some energy from the impact plate. This foam is absent in FE model. For a better agreement of FE model with the steering wheel, FE model may need to be stiffer. Modeling of foam around the steering wheel can be the other alternative.

Key words: He*avy vehicle steering wheel, Frontal crash, Impact test-setup, Physical testing and simulations, Rim tilt angles, Contact force, Rim deformation, FE model validation.*

Contents

Preface

The current thesis work was performed at SAFER; vehicle and traffic safety center at Chalmers, Lindholmen campus, Gothenburg. This thesis work was for the Master degree in Automotive Engineering at Department of Applied Mechanics in Chalmers University of Technology. It was a joint venture of Chalmers University and Volvo 3P. The supervisor at Chalmers was Kristian Holmqvist; PhD Student at the division of Vehicle Safety, and Peter Rundberget; Feature leader at Volvo 3P, Cab Engineering. The examiner was Assistant Prof. Karin Brolin; Division of Vehicle Safety. The authors are highly grateful to the supervisors in special and the examiner in general for their help and concern to accomplish this thesis work.

Construction of the physical test setup was performed at Prototype Workshop in Applied Mechanics department at Chalmers. The authors would like to acknowledge Morgan Svensson, without his dedication and prioritizing the test setup construction; this could not be possible to end the thesis work on time. Physical testing was performed at Chalmers. We would like to express our high gratitude to all the officials and staff members who been very helpful during the physical testing.

We would also like to thank all the other people who have been supportive throughout our thesis work.

Gothenburg December, 2011

Anees ur Rehman

Mehdi Esmaieli Najafabadi

1 Introduction

A high portion of the severe thoracic injuries in drivers of heavy vehicles, subjected to a frontal crash are believed to have been caused by chest contact to the steering wheel rim. This thesis focuses on defining relevant methods for model development in Finite Element (FE) modeling for an already existing model of truck steering wheel. An impact test setup is identified for the current thesis work, and will be used to evaluate the behavior of steering wheel under different loading conditions. Moreover, the study focuses on designing and building a physical test setup to support the FE methods. The FE code used is LS-DYNA® (Hallquist, 2007).

1.1 Background

Heavy vehicles in Sweden are involved in about 20% of the traffic accidents that cause occupant fatalities (Lundqvist *et al*., 2010). Although the heavy vehicles represent less than 10% of the traffic, but due to their heavy weight of about 18 tons, the crashes are violent and consequences are severe (Lundqvist *et al*., 2010). In the recent decades, more efforts are carried out in order to reduce the number of killed occupants per travelled kilometer, by increasing the driver's and heavy vehicles safety (Lundqvist *et al*., 2010). As a result, the number of people killed and injured in traffic accidents has declined dramatically since 1953 (Lundqvist *et al*., 2010).

In heavy commercial vehicles, low safety belt usage among the drivers has been reported, which is believed to increase the risk of steering wheel rim to chest contact in frontal collisions. The seating posture and the cabin's geometry of the heavy vehicles change the situation of the driver as compared to the passenger car drivers. Cabin's geometry changes the position of the back of seat; it is more upright compared to driver seat in passenger cars. In the event of a frontal crash in a heavy vehicle, these differences increase the risk of steering wheel rim to upper body contact (Gwehenberger *et al*., 2002) which means that the driver of a truck is at risk of sustaining severe thoracic injuries (Sukegawa *et al*., 2001).

A risk of severe injuries from the steering wheel rim to thorax contacts has been identified in vehicle frontal collisions (Holmqvist *et al.,* 2010). Hybrid III crash test dummy is used to evaluate biomechanical responses in heavy vehicle frontal crash (Holmqvist *et al.,* 2009). It was mainly developed for use in passenger cars and the load cases most common to them. At the time of the Hybrid III's development, the loading pattern of the chest was from the hub of the center steering wheel and not the rim (Holmqvist *et al.,* 2009). To further advance in truck safety, without developing new dummies, it is necessary to know how to use the dummy properly for a load case found in trucks i.e. with a possible rim impacting the thoracic area.

Steering wheel adjustability at different tilt angles for the ease of driver to handle steering wheel, adds to several load cases to chest, during impact. Hybrid III chest was found more sensitive to changes in impact at different steering wheel tilt angles than the human body model THUMS (Holmqvist *et al.,* 2010). A set of angles can be selected, to see sensitivity of steering wheel tilt angles in impact. There is a need therefore, to analyze the crashes and injuries to heavy vehicle drivers; hence a model of a steering wheel will be developed and validated from a basic FE model, with the use of physical test results.

1.2 Objective

The main aim of this thesis work focuses on validation of an already existing FE steering wheel model. Identification of an appropriate design test setup and replicate the design, both in physical testing and FE modeling. A set of four different loading cases will therefore be selected, based on tilt angles of the rim. The data from accelerometers, load cells and high speed video will be collected and analyzed to validate the FE model.

2 Methodology

A need for an impact test setup was identified for the current steering wheel model validation. The impact test setup was designed and the same setup was replicated both for the physical testing and FE modeling. The impact object was adjusted to impact the steering wheel at different tilt angles of the rim. The object was set to a velocity of 5 m/s, which is the relative velocity of belted driver to the steering wheel in a 30 km/h delta-v crash (Holmqvist *et al.,* 2010). The rim loading was also modeled in FE environment. Simulations were performed for the model in LS-DYNA. Force-displacement response was obtained both from physical tests and simulations.

2.1 Designing physical test setup

The impact test setup was designed in CATIA V5 R21® (Dassault Systemes, 2010), and then replicated both in physical test setup and FE. The test set up for the steering wheel is shown in Fig. 2.1. The basic principle was to utilize the rubber cords (not shown in Fig.) energy to propel the sled. The center of the hub was fixed with a steel shaft. A vertical beam was mounted on the sled to impact the steering wheel. From now and onwards, this impact beam will be called as the impact plate. The velocity of impact was calibrated for a mass of 35 kg of the sled-plate assembly. Two load cells each of 10 kN load capacity, were installed parallel to the direction of the impact force. These load cells were equidistant from the impact point. The steering wheel was tested at different tilt angles of the rim, so the shaft fixture was designed flexible. Horizontal beam also had the flexibility of moving up and down through the two vertical slots, used to keep the load cells equidistant from the contact point while testing for different tilt angles.

A rubber stopper was placed to prevent the damage to the load cells, due to collision of impact plate with the shaft fixture. Any contact of impact plate with the hub or shaft fixture due to the rim bending about Y-axis was undesirable.

The friction force produced due to contact of impact plate and the rim, may damage the load cells. It must not be more than 5% of the load cells capacity. The surface on the impact plate around the contact area was finished properly to reduce the friction force.

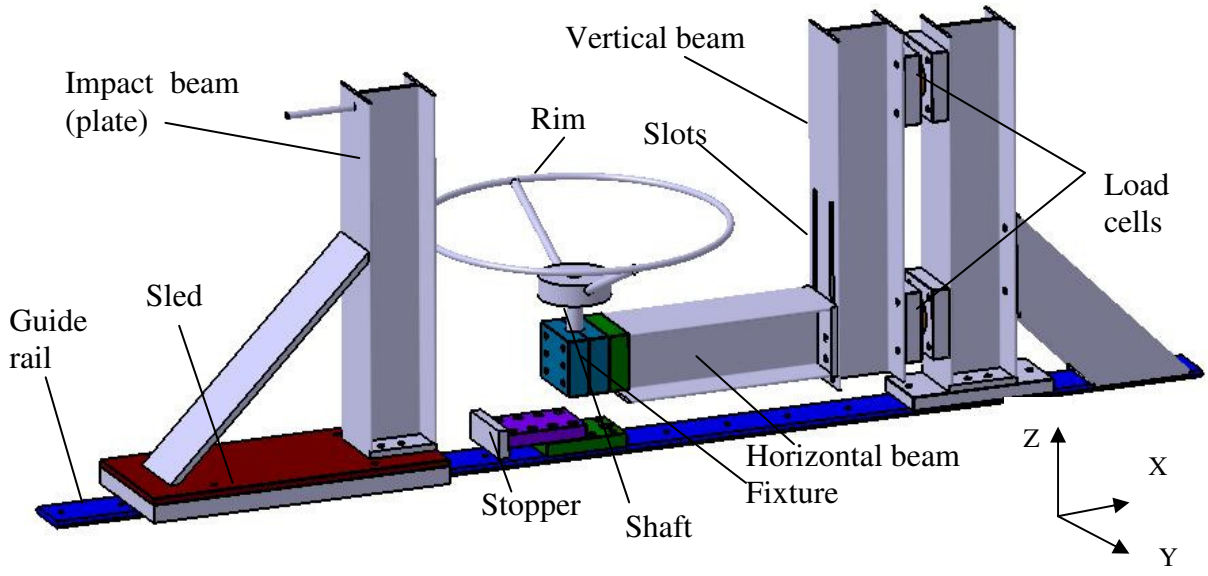

Fig 2.1 Test setup design, 0 degree tilt angle (Front view)

2.1.1 Designing physical test setup for different tilt angles

Load cases for testing steering wheel were based on the tilt angle of the rim. A rectangular steel block with 10, 20 and 30 degree wedge angle was replaced each time, in order to tilt the steering wheel rim to the same angle. Fig 2.2 shows the design for physical test setup for 10 degree tilt angle of the rim.

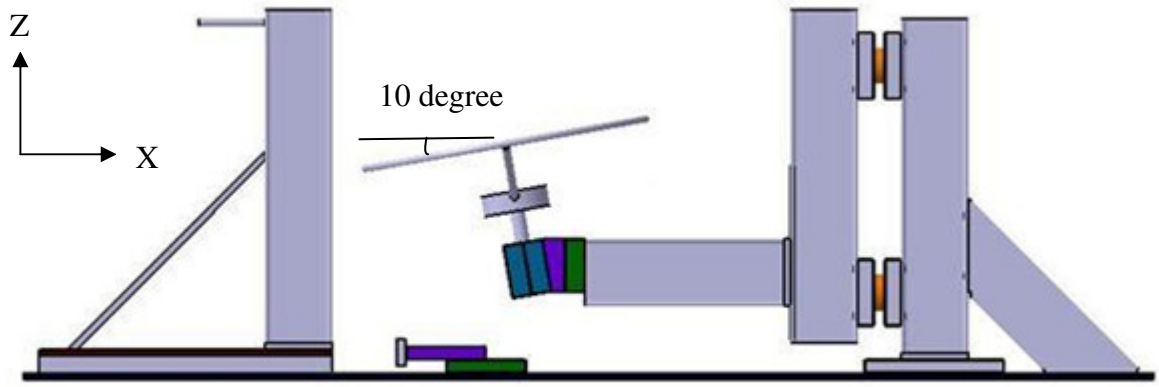

Fig. 2.2 Test setup design for 10 degree tilt angle

2.1.2 Energy balance

The energy balance for the test setup is shown in Fig. 2.3.

The impact force is equal to the force measured by the two load cells. Since, the contact point was equidistant from the load cells, so in the absence of any friction force at the contact point, the measured force by each load cell is equal to the half of the contact force. Due to the friction force at contact, a moment about Y-axis can be created. This would change the force reading of the two load cells, and they are not equal anymore.

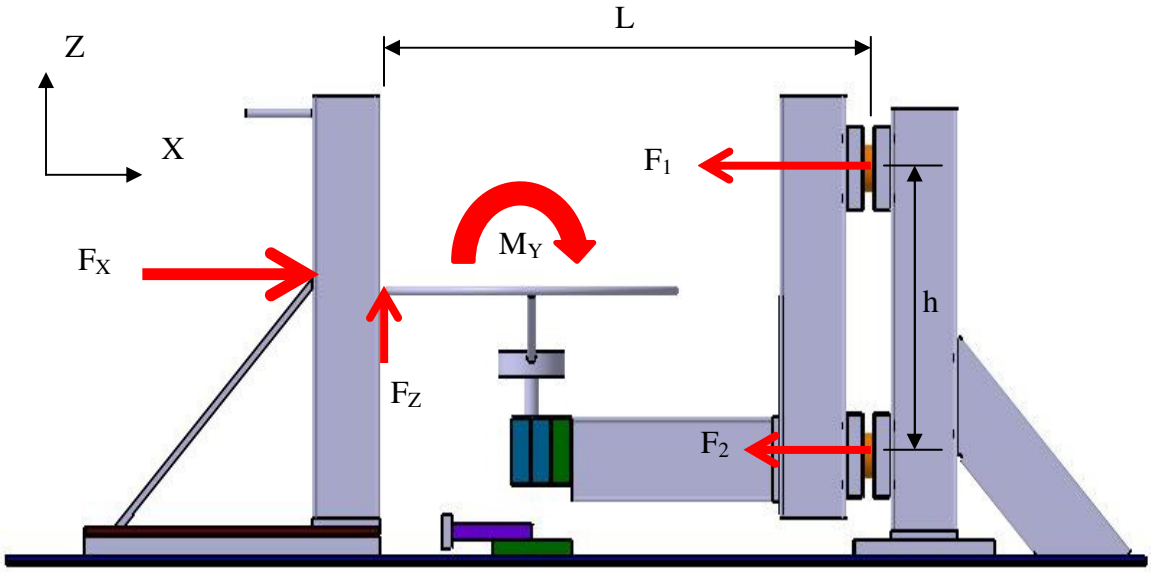

Fig. 2.3 Energy balance for test setup

From the figure, Impact force, F_X = Force Load cell top(F_1) + Force load cell bottom (F_2)

Moment about Y-axis, $M_Y = F_z * L = (F_1 - F_2) * \frac{h}{2}$

For $F_z = 0$, $M_Y = 0$ and $F_1 = F_2$

2.1.3 Assumptions

Some assumptions were considered before performing the physical testing of the steering wheel. The friction between the sled and the rail after the impact was ignored. The energy losses due to heat or noise were also ignored. This means whole kinetic energy of the sled-plate assembly was used to deform the rim during the impact. Effects of the air resistance were also assumed to be very low that they cannot influence the results.

2.1.4 Equipment used

Four rubber cords were used to pull back the sled to the calibrated distance against the restoring force and lock the sled in position. Other equipment used is:

Force transducers:

Two force transducers Model 8524 (Interface) were used to estimate the impact force applied by the impact plate to the steering wheel. Due to their compact design and construction, these tension-pressure load cells can be operated without any problems in any loading environments.

Accelerometers:

An accelerometer Model 11054 (ENDEVCO) was glued to the body of the sled. This gave the acceleration of the plate after the impact. The input data was stored in voltage changes and later used in brick software. Another accelerometer Model A014943 (ENDEVCO) was used to measure the acceleration of the structure after the impact, so the total acceleration will be the absolute value of acceleration from the two accelerometers. By multiplying the mass of sled-plate assembly with the absolute acceleration, force level was obtained. This force level was compared to the force obtained from the two load cells.

High speed camera:

A high speed camera Kodak EktaPro RO imager was used to observe the displacement of impact plate.

Focal length of the lens: 65 mm, aperture: f/2.8 shot at 1000 frames per second.

Data acquisition:

All the data from sensors was stored in GMH Engineering BRICK, which is used for managing the hardware and reading the data. Calibration factors were set in order to get exact reading from the load cells and accelerometers. The time in which the brick records the data from the sensors is an important parameter. After recording the data, it can be uploaded from the brick and after post processing, the data can be saved as a text file which can be imported to excel sheet for filtering and removing mechanical noises. The data was filtered using filter SAE CFC 50. The sampling frequency for the data from accelerometers and the load cells is 1373 Hz, and for the camera it's 1000 Hz.

2.1.5 Procedure

Two tests were performed for each tilt angle, 0, 10, 20 and 30 degree. A specially designed fixture was used for the steering wheel shaft to hold it firmly and to provide a support, so during the impact it should not show any bending. Two markers were placed on the impact plate at a vertical distance of 400 mm, all the video analysis was based on this measurement. Markers were also placed on the steering wheel rim at the point of impact and on the other side of rim, to see how much the rim deformed or bent on impact. The tests performed for

different load cases are shown in Table 2.3, which shows the impact object and the steering wheel tilt angle.

Table 2.1 Physical testing at different tilt angles

Test No.	Tilt angle of the rim	Target object
1	0	Steering wheel rim
2	0	Steering wheel rim
3	10	Steering wheel rim
4	10	Steering wheel rim
5	20	Steering wheel rim
6	20	Steering wheel rim
7	30	Steering wheel rim
8	30	Steering wheel rim

2.2 FE steering wheel model

Current model of the steering wheel already existed in LS-DYNA code. It was originally developed using PAM-CRASH (ESI Group, France) code, and then translated to the LS-DYNA. All the material and geometric properties used were assigned by the manufacturer. The FE model did not have the foam around the rim and spokes. The model was simplified to reduce the CPU calculation time.

2.2.1 Geometry and the mesh

Fig 2.4 shows the FE model of the steering wheel. The model has a circular rim of 433 mm outer diameter. The rim had a hexahedral mesh. Other components of the steering wheel include a pair of rear and the front spokes. The rear spokes have the diameter 6 mm, and the front spokes have the diameter 8 mm. Both the rear and the front spokes were also assigned a hexahedral mesh. Spokes are used to connect rim with the hub. The hub is the part of the steering wheel at the center. It joins the steering wheel to the shaft and transmits the torque from the steering wheel rim to the shaft. The hub had more refined tetrahedral mesh.

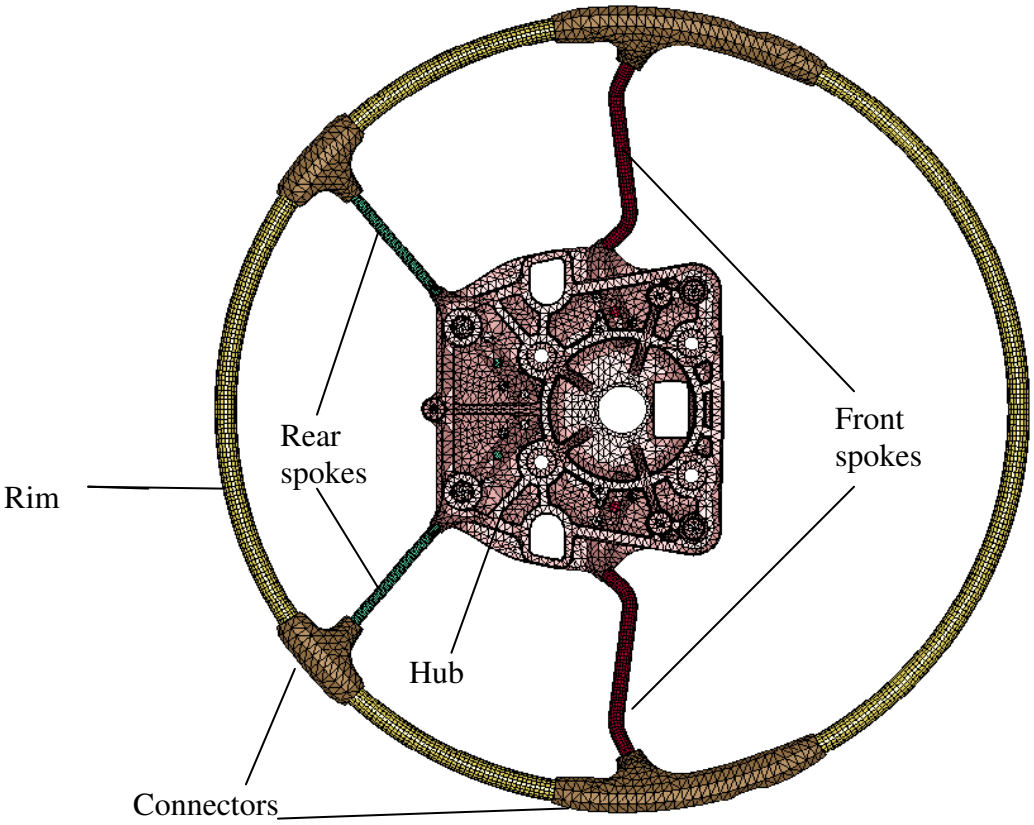

Fig. 2.4 FE steering wheel model

2.2.2 Material

The material properties of steering wheel components are listed in Table 2.2. Material cards presenting the parameters of plasticity for different components are shown in Appendix A.

Table 2.2: Material properties of steering wheel parts

Component	Element	Material model	Young's modulus	Poisson's ratio
Rim	Shell	Piecewise Linear Plastic	192 GPa	0.3
Rear spokes	Solid	Piecewise Linear Plastic	196 GPa	0.3
Front	Solid	Piecewise Linear Plastic	200 GPa	0.3
Hub	Solid	Piecewise Linear Plastic	40 GPa	0.3
Connectors	Solid	Piecewise Linear Plastic	40 GPa	0.3

2.2.3 Simulations of the test setup

Fig. 2.5 shows the replication of designed impact test setup of the steering wheel model in FE. In order to represent the fully constrained steering wheel column, the central portion of the hub was constrained for all translations and rotations. The steering wheel model was impacted with a rigid solid steel plate of 100*100 mm size with a thickness of 10 mm, at velocity of impact 5 m/s, with 0 degree steering angle position. A surface to surface contact

was defined between the plate and the steering wheel rim with friction coefficient of 0.3. The plate was made fully constrained except for X-axis translation. The density of the plate was selected to get a mass of 35 kg. An accelerometer was also modeled at the center of the rigid plate, in order to get the accurate measurement of acceleration of plate. The accelerometer reduces the numerical noise, and gives better results than results extracted directly from a node. The measured force by the two load cells during physical testing was compared to the contact force during simulation. Similarly, the displacement of the impact plate was also compared.

(a) Steel plate impact with the steering wheel *(b) Fully constrained hub at center*

Fig. 2.5 FE test setup for the steering wheel

Simulations were also performed for testing steering wheel at different steering angle positions. Steel plate was impacted to the rim at the positions where spokes were located. In Fig. 2.6, a nomenclature is explained for testing steering wheel at different steering angle positions.

No.	Angles	Definition
1	Angle 0	Steering wheel with 0 degree steering angle
2	Angle 1	Steering wheel with 35 degree steering angle (Rear spoke)
3	Angle 2	Steering wheel with 85 degree steering angle (Front spoke)

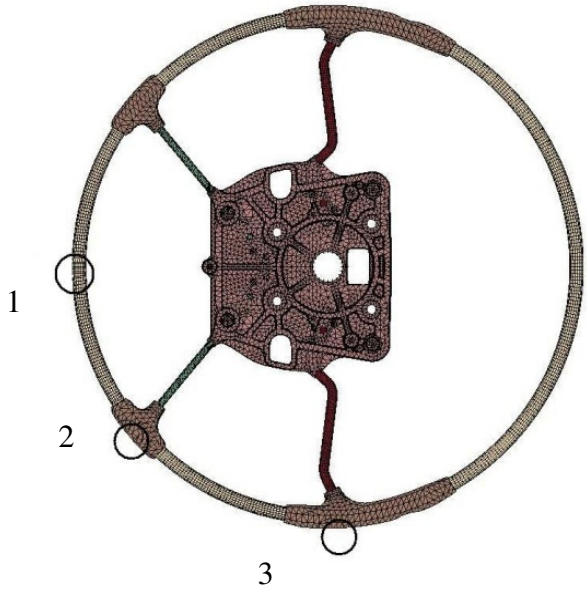

Fig 2.6 Steering angle positions

2.2.4 FE setup for testing steering wheel at different tilt angles

FE test setup for testing steering wheel model at different tilt angles of the rim at the time of impact is shown in Fig. 2.7.

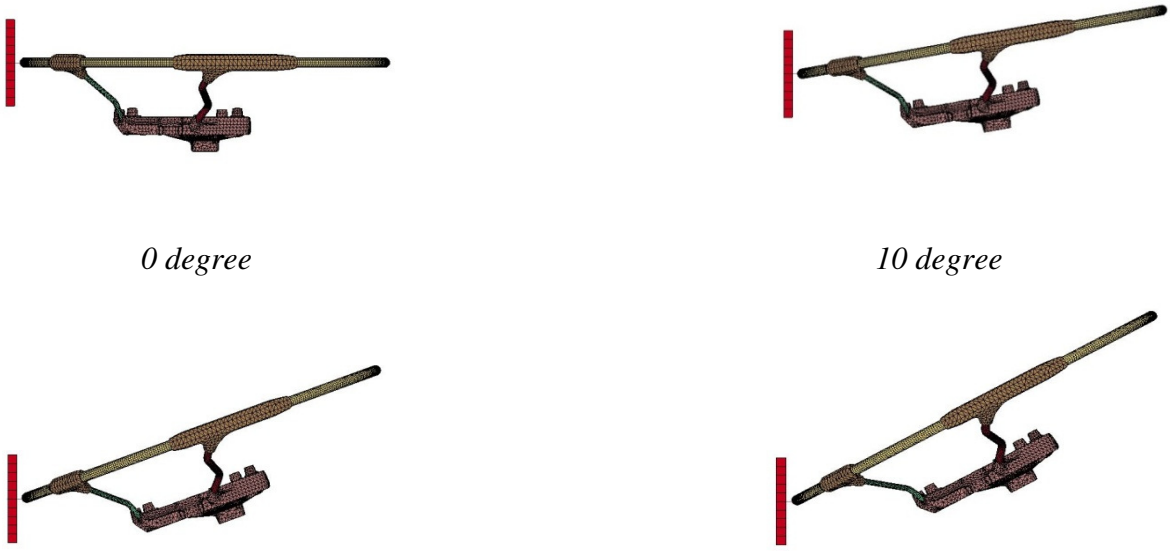

0 degree *10 degree*

20 degree *30 degree*

Fig 2.7 Tilt angles of the rim

2.3 Body block model

In addition to the impact test of the steel plate against the steering wheel, a body block model was also impacted to the steering wheel. Fig. 2.8 shows body block impact with the steering wheel. The body block model already existed in LS-DYNA code. Originally it was developed in Radioss ^{TM} (Altair Radioss v10, 2009) and then translated to LS-DYNA. Physical tests for the model were previously performed at Volvo car safety center. Simulation results for the body block model are to be compared to the test results.
The mass of the body block is 36 kg, which is the mass of 50th percentile torso-shaped body block according to ECE R12 regulation. The body block impacted the steering wheel rim at a speed of 5.25 m/s (According to ECE R 12 regulation, except for speed), and a rim tilt angle of 10 degree, based on in-house Volvo testing. Simulations were also performed for steering angle positions, Angle 1 and Angle 2 as shown by Fig. 2.6. An accelerometer was modeled at the center of gravity similar to the physical body block. A force-displacement response was obtained for further analysis.

The geometric and material properties of the body block model are presented in Table 2.3. The material card for the body block showing the parameters of the plasticity is shown in Appendix A.

Table 2.3 Geometric and material properties of the body block

Mass kg	**Element type**	**Material model**	**Density kg/mm^3**	**Young's modulus GPa**	**Poison's ratio**
36	Shell (10 mm thick)	Simplified Johanson Cook	$7.85*10^{-6}$	207	0.3

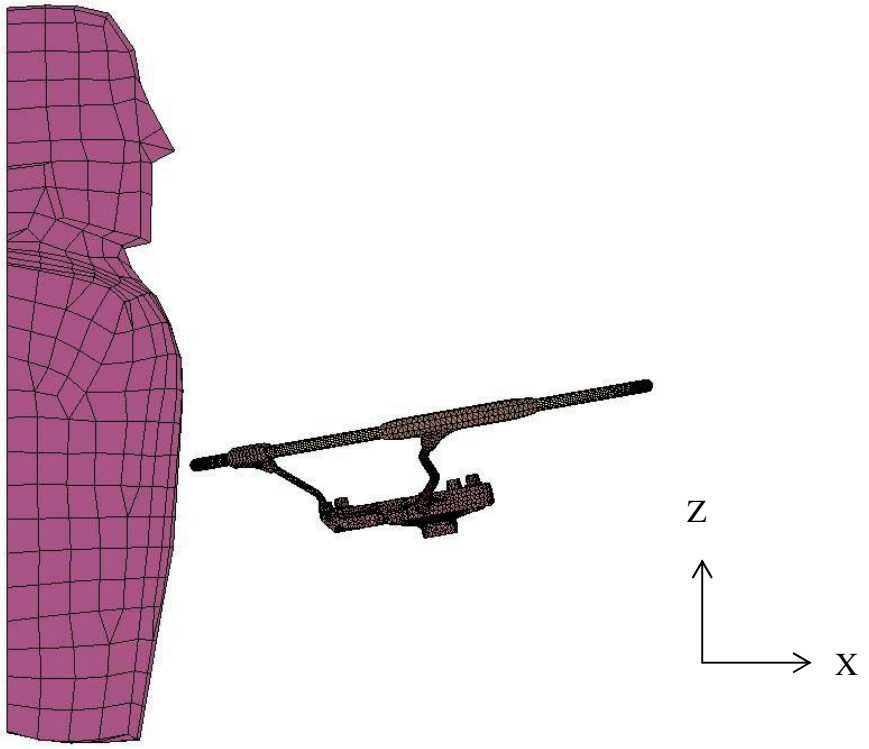

Fig 2.8 Body block impact with steering wheel

3 Results

Results are presented in the following section both for physical tests and simulation.

3.1 Physical tests

Two tests for each tilt angle were performed. Velocity of impact was one of the important parameters, and determines the amount of energy carried by the plate. The sled was pulled to a certain distance to achieve a velocity of impact 5 m/s. However, this velocity of impact was found to be lower than 5 m/s. In Table 3.1, velocity of impact for all the tilt angles during physical testing is presented.

Table 3.1: Velocity of impact for four tilt angles (units in m/s)

0 degree		10 degree		20 degree		30 degree	
Test 1	Test 2	Test 3	Test 4	Test 5	Test 6	Test 7	Test 8
4.79	4.51	4.81	4.55	4.83	4.59	4.90	4.59

3.1.1 Test 1 and 2

Horizontal displacement of impact plate

The horizontal displacement of the plate was only considered after the contact initiated. This way the deformation of the rim can also be estimated.

Impact plate horizontal displacement for the two tests for 0 degree tilt angle is shown in Fig. 3.1 (a). After the impact initiated, the horizontal displacement of the impact plate in both the tests was similar. For Test 1, the plate continued its displacement until the rim collided the horizontal support beam due to its bending about Y-axis. This was due to temporary emergency stopper failure.

For Test 2, the plate hit the stopper. This reduced the velocity of impact plate until the plate rebounded back. The stopper prevented the rim collision with horizontal support beam after the bending. Maximum horizontal displacement the impact plate moved before its rebound was 17% less than Test 1. Similarly, the final rim deformation in Test 2 was found 36% lower than Test 1.

Contact force

Contact force against the horizontal displacement of impact plate for both the tests is presented in Fig. 3.2 (a). During Test 1, the rim due to its bending about Y-axis, collided the horizontal support beam, a sudden peak was expected. At this point, the velocity of impact plate observed was ~1 m/s. A small rise in force level from load cells was observed, but due to filtration it is not apparently visible.

For Test 2, the impact plate hit the rubber part of the stopper after 15 ms of impact. The rubber part of the stopper is 20 mm thick, and absorbed the energy from the impact plate until it was fully compressed. After its compression, the loading from the plate was taken up by the steel part of stopper. At this point, the whole structure moved and a sharp rebound was observed, that can be seen in the force curve from the load cells result. Maximum force level observed was 16% less than Test 1.

From accelerometers, force level in Test 1 reached to its maximum value nearly the same as the corresponding force level obtained from the load cells. In Test 2, as the impact plate hit

the stopper, a sharp rise in accelerometers reading was observed. Maximum force obtained was almost the three times the force level obtained from the corresponding load cells.

3.1.2 Test 3 and 4

Horizontal displacement of impact plate

Impact plate horizontal displacement from Test 3 and Test 4 for 10 degree is shown in Fig. 3.1 (b). The rim showed deformation and also slight bending about Y-axis. Due to reduced kinetic energy of the plate during Test 4, the maximum horizontal displacement of the impact plate was 20% lower than Test 3. Similarly the final rim deformation for Test 4 was found 47% lower than Test 3.

Contact force

Contact force for Test 3 and Test 4 against impact plate displacement is presented in Fig. 3.2 (b). From the load cells result, maximum force level observed for Test 3 was 7% higher than Test 4.

From the accelerometers results, maximum contact force for Test 3 was 6% higher than the corresponding load cells result. Similarly, for Test 4, the maximum contact force observed from the accelerometers was 14% higher than the corresponding load cells result. However, the accelerometer force results from both the tests were found nearly similar.

3.1.3 Test 5 and 6

Horizontal displacement of impact plate

Impact plate horizontal displacement for Test 5 and Test 6 is shown in Fig. 3.1 (c). Higher rim deformation and slight rim bending about Y-axis was observed. For Test 5, rupture of foam was observed around the rear spokes. For Test 6, impact plate reached to its maximum horizontal displacement with 24% lower value compared to Test 5. Similarly, final rim deformation observed was 28% lower than Test 5.

Contact force

Contact force results from the two tests are shown in Fig. 3.2 (c). The curves show that after the contact initiated, force level for Test 6 started to rise earlier than Test 5. However, due to lower energy of the impact plate (because of low impact velocity), maximum force level in Test 6 was observed at an earlier displacement than in Test 5. For Test 5, maximum force value observed was 6% higher than Test 6. Force level from both the curves was observed to fall prior to maximum horizontal displacement.

From the accelerometer results, for Test 5, maximum force level obtained was 3% higher than the corresponding load cells result and is not a significant difference. From Test 6, maximum force level observed was 9% higher compared to the corresponding load cells result. However, this result is almost the similar as the accelerometers result in Test 5.

3.1.4 Test 7 and 8

Horizontal displacement of impact plate

Fig 3.1 (d) shows the impact plate displacement for the two tests. Similar to 20 degree tilt angle, higher rim deformation was observed. Bending of the rim around Y-axis was found almost negligible. For Test 7, the impact plate reached to a maximum horizontal displacement 12% higher than Test 8. Final rim deformation observed was 10% higher than Test 8.

Contact force

Contact force for the two tests is shown in Fig. 3.2 (d). For Test 7, maximum force level observed was 10% higher than Test 8. Rupture of foam was also observed around the rear spokes during Test 7.

From the accelerometers result, for Test 7, maximum force level observed was nearly the similar as the corresponding load cells result. Similarly, for Test 8 from the accelerometers result, the maximum force observed was 5% higher than the corresponding load cells result.

3.2 Simulation results

Simulation data was filtered with SAE CFC 50. The data extracted is for the first 50 ms.

3.2.1 0 degree tilt angle

Horizontal displacement

Fig 3.1 (a) also shows the impact plate horizontal displacement for 0 degree simulation. This horizontal displacement is taken in the normal X-axis direction.

After the impact, sliding of the rim was observed that produced the friction force. This friction force caused the rim to bend about Y-axis. Due to the rim sliding and bending, steering wheel hub was exposed to the impact plate. The impact plate reached the hub of steering wheel after 27 ms of the impact. There was no contact defined between the plate and the hub, so there was no rebound of the impact plate, and it continued to move even after reaching the hub.

Contact force

Contact force result for 0 degree simulation is shown in Fig. 3.2 (a). 0 degree tilt angle had the lowest force level in the elastic region than all the other tilt angles. After the elastic deformation of the rim, a drop in force level was observed. The force reading was only considered till the plate reached the hub of the steering wheel.

3.2.2 10 degree tilt angle

Horizontal displacement

Impact plate horizontal displacement for 10 degree simulation is shown in Fig. 3.1 (b). Similar to 0 degree tilt angle, the rim also showed bending about Y-axis. The impact plate had the least displacement than all the other three load cases; however this difference was not significant. After plate reached to its maximum displacement, it rebounded back.

Contact force

Contact force result for 10 degree is shown in the Fig. 3.2 (b). 10 degree tilt angle had the maximum force level than all the other load cases. Due to the position of the rim, it showed a higher resistance to the impact plate.

3.2.3 20 degree tilt angle

Horizontal displacement

Impact plate horizontal displacement for 20 degree simulation is shown in Fig. 3.1 (c). For 20 degree tilt angle, higher rim deformation was observed than rim bending. The impact plate after deforming the rim reached to a maximum displacement value of 2% higher than 10 degree tilt angle. Plate also rebounded after reaching its maximum displacement value.

Contact force

Contact force result for 20 degree simulation is shown in the Fig. 3.2 (c). The force response was steady after the initial rise and ended up with the maximum force level 20% lower than 10 degree tilt angle.

3.2.4 30 degree tilt angle

Horizontal displacement

Impact plate horizontal displacement for 30 degree simulation is shown in Fig. 3.1 (d). Similar to 20 degree, higher rim deformation was observed, and the rim bending about Y-axis was almost negligible. The impact plate had 9% and 6% higher displacement than 10 and 20 degree. After reaching to its maximum displacement, plate started to rebound. It is notable that the impact plate did not reach the hub as it reached during 0 degree tilt angle. The horizontal distance between the contact point and the hub for 0 degree is 107 mm, whereas for 30 degree tilt angle, this distance is 129 mm.

Contact force

Contact force result for 30 degree is shown in the Fig. 3.2 (d). The force level dropped gradually after the initial rise, and ended up with the force level 40% lower than 10 degree tilt angle, and then started to rebound.

3.3 Comparison of the results

A comparison of the results from physical testing and simulation for four tilt angles is presented in the following section. This comparison is presented for the impact plate displacement and the force level from the load cells only.

3.3.1 0 degree tilt angle

During the simulation, the impact plate reached the steering wheel hub after 27 ms of the impact, so results for the impact plate displacement and the force level, both from the simulation and the physical tests were compared for this period only.

Fig 3.1 (a) also presents the comparison of the physical tests and the simulation result for impact plate horizontal displacement.

From the physical Test 1, sliding of the rim in positive Z-axis and the rim clockwise bending about Y-axis was observed. Similar sliding and bending was also observed during simulation. Due to this bending, the rim collided with the horizontal beam after 30 ms, and the impact plate was about to hit the hub of steering wheel. For 27 ms after the impact, the horizontal displacement of the impact plate during simulation was found 22% higher than Test 1.

Final deformation of the rim during simulation was found 50% higher than Test 1.

In Test 2, in order to avoid the rim collision with the horizontal support beam, the stopper on the guide rail was placed 30 mm to the left from its position. The impact plate hit the stopper, and restricted its motion. Horizontal displacement of the impact plate during simulation was found 42% higher than Test 2.

Final deformation of the rim during simulation was nearly the similar as Test 2.

Comparison of the force level for the two physical tests and simulation during 0 degree tilt angle is shown in Fig. 3.2 (a).

For 27 ms, force level for simulation was nearly the similar as Test 1, whereas it was found 27% higher than Test 2. The reason for this difference was the impact of plate with the rubber

stopper that carried most of the energy of the plate. This lowered the force reading from the load cells.

3.3.2 10 degree tilt angle

Fig. 3.1 (b) shows the analysis of impact plate horizontal displacement during physical tests and simulation for 10 degree tilt angle.

Deformation of the rim and bending about Y-axis was observed during both physical tests and simulation. Horizontal displacement of the impact plate during simulation was found 25% higher than Test 3. Final deformation of the steering wheel rim during simulation was found 54% higher than Test 3.

Lower horizontal displacement of impact plate was observed in Test 4 as compared to simulation. For simulation, it was 57% higher than Test 4. Final rim deformation during simulation was 128% higher than Test 4.

Fig. 3.2 (b) shows the force level comparison for the two physical tests and simulation. Force level for simulation ended up in the same range at Test 3, and was 8% higher than Test 4.

3.3.3 20 degree tilt angle

Physical test results for impact plate horizontal displacement are compared to the simulation for 20 degree tilt angle and are shown in Fig. 3.1 (c).

During the physical tests and simulation, lower bending and higher rim deformation was noticed. However, deformation of the rim during simulation was higher than the physical tests. For simulation, the impact plate horizontal displacement was 25% and 65% higher than Test 5 and Test 6 respectively. Similarly, the final deformation of the rim observed during simulation was, 53% and 96% higher than Test 5 and Test 6 respectively.

Fig. 3.2 (c) also shows the contact force comparison of two physical tests and simulation.

For simulation, force level after the impact initiated, appeared to rise earlier than the physical tests. However, the rim deformation was found higher than the physical tests, and force level remained more or less steady after the initial rise. Whereas, physical test results followed the same typical curve as for 0 and 10 degree tilt angles. As a result, the maximum force level for simulation was found 26% and 21% lower than Test 5 and Test 6 respectively.

3.3.4 30 degree tilt angle

Physical test results for impact plate horizontal displacement along with simulation for 30 degree tilt angle is presented in Fig. 3.1 (d).

The rim deformation during simulation was found higher than the two physical tests. As a result, the impact plate displacement was also higher than physical tests, and it was 30% and 47% higher than Test 7 and Test 8 respectively. Similarly, the final rim deformation was found 56% and 75% higher than Test 7 and Test 8 respectively.

Fig. 3.2 (d) shows contact force comparison of the physical tests and simulation.

Force level for simulation was found quite lower than the physical tests. Soon after the impact, force level for simulation reached the peak value and then continued to fall. Physical tests had the typical curves like all the other tilt angles. Before the rebound, force level during Test 7 was found 45% higher than the simulation, whereas for Test 8, it was 31% higher than the simulation.

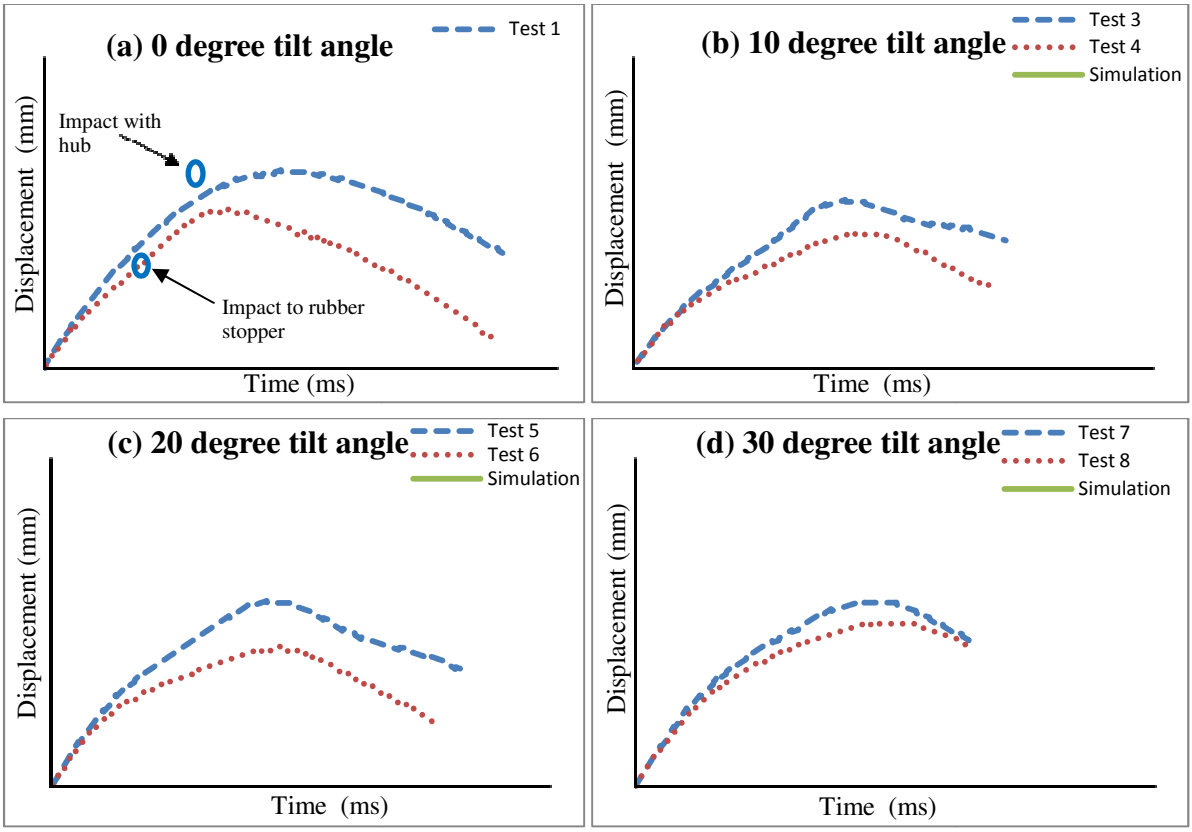

Fig. 3.1 Horizontal displacement of impact plate

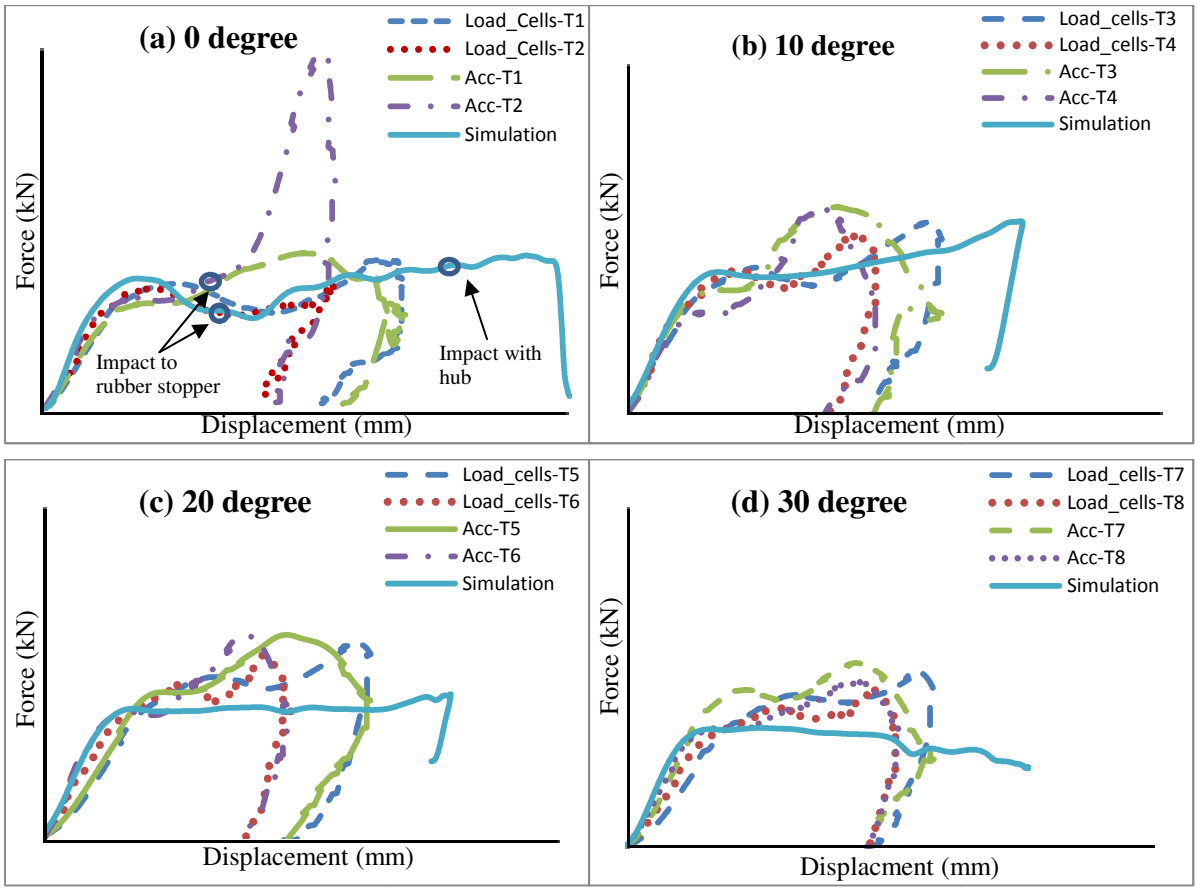

Fig. 3.2 Contact force

3.4 Body block

3.4.1 Physical testing

Physical tests for body block were performed at Volvo car safety center. The results are presented for X-torso force and resultant force for the impact at three different locations of the rim. These results were already presented by Volvo car safety center. The filter used was SAE CFC 180.

Angle 0

Physical test results for Angle 0 position are shown in Fig. 3.3 (a).

From the movie results, it was found that front of the body block was not rigid and deformed elastically by the rim. The rim also hit the fixture at the other end. This gave more resistance to body block and reduced its displacement, consequently lowered the rim deformation and raised the X-torso force, after a fall from the initial rise.

Angle 1

Physical test results for Angle 1 position are shown in Fig. 3.3 (b).

Body block impacted the rim where rear spoke was located. Due to spoke, higher resistance was observed. The rim showed bending after the initial rise in X-torso force. The rise in resultant force is at a different body block displacement and maximum force level observed was 8.52 kN. Moreover, front of body block was deformed elastically by the rim. Similar to Angle 0, the rim also hit the fixture, and was constrained of any further bending. This ceased the body block displacement. As a result, a rise in X-torso force was observed after the drop from initial rise. This rise can also be seen in resultant force after fall from the maximum level.

Angle 2

Physical test results for Angle 2 position are shown in Fig. 3.3 (c).

The body block impacted the rim where front spoke was located. Similar to rear spoke, higher resistance was observed from the front spoke. The peak value for resultant force observed was at a different displacement than the X-torso force. A fall in force level was observed after the peak values both for the X-torso force and resultant force. The rim showed bending and hit the fixture, which raised the force levels again. Maximum displacement for the body block was 104 mm. X-torso force appeared to fall prior to the maximum displacement of the body block.

3.4.2 Simulation

Simulation results for the body block were extracted and presented below. Results are shown for the force in X-direction and the resultant force. However, the X-force and resultant force results are more or less similar. The filter used was SAE CFC 180 in accordance with the previously performed tests at Volvo.

Angle 0

Contact force for body block impact at Angle 0 position is shown in Fig. 3.3 (a). On Impact, the rim bending about the Y-axis and its deformation was observed. The contact force gradually reached the maximum force level after the elastic zone.

Angle 1

Contact force for body block impact at Angle 1 position is shown in Fig. 3.3 (b). Soon after the impact, force level reached to the maximum value remained steady afterwards until the rebound of the body block. The spoke also showed bending and deformation, and collided the hub of the steering wheel.

Angle 2

Contact force against body block displacement for impact at Angle 2 position is shown in Fig. 3.3 (c). Higher resistance to impact was observed by the front spoke compared to the rear spoke. Contact force after the impact, reached to the maximum value. Force level dropped afterwards and remained steady, until the body block started to rebound. Similar to the rear spoke; front spoke also deformed plastically and collided with the hub.

3.4.3 Comparison of the results

Fig. 3.3 also shows the comparison of the results from both the physical tests and simulations. It is important to mention that physical tests were performed on a vertical test rig, and the body block used during the physical testing was a rubber body block, with 1 mm thick steel plate in front, around the contact area. For simulation, a horizontal test setup was considered, and results from simulation do not include the gravity effects. The FE model also did not pass the calibration test; hence the front of the body block was more or less rigid.

Angle 0

A comparison of simulation and physical tests for the impact of body block at Angle 0 position is shown in Fig. 3.3 (a).

During physical testing, due to elastic deformation of the front of body block, the initial rise in force level was found at a different displacement than simulation. The rim also impacted with the fixture at the other end. This gave more resistance to body block and reduced its displacement, consequently reduced the rim deformation and raised the force level. Comparatively during simulation, due to more deformation of the rim, higher displacement and lower force level was observed.

Maximum force level achieved for simulation results was 16% lower than the X-torso force of the physical test. Whereas, maximum displacement achieved by the body block was 9% higher in simulation.

Angle 1

A comparison of physical tests and simulation for Angle 1 position is shown in Fig. 3.3 (b). During simulation, the initial resistance to deformation caused a higher peak force. The force level at this peak for simulation was almost the similar as the corresponding initial rise in force level during testing. Out of plane bending of the rim in X-axis as well as in Y-axis was seen, therefore force level dropped from the initial peak value.

During testing, after the initial rise in X-torso force, the rim showed some bending. Moreover front of the body block was deformed elastically by the rim. This caused the rise in force level at different body block displacement than simulation. The rim hit the fixture, and before the rebound, force level was 29% higher than simulation. Maximum displacement of the body block was nearly the similar both for the simulation and physical test, i.e. 104 mm.

Angle 2

Fig. 3.3 (c) shows the comparison of simulation and physical tests for Angle 2 position. From the simulation results, it was observed that after the impact, front spoke resisted the body

block motion, and out of plane bending of the rim was observed both in X-axis and Y-axis. Due to high resistance offered by the spoke, force level shoot up to a maximum value 25% higher than the maximum X-torso force.

From the movie for physical testing, it was observed that the structure was not too rigid and the whole structure moved on impact. Similar to impact at Angle 0 and Angle 1, front of body block deformed elastically and resulted in maximum force at a different displacement than simulation. Due to this elastic deformation, displacement for simulation was found 25% lower than physical tests.

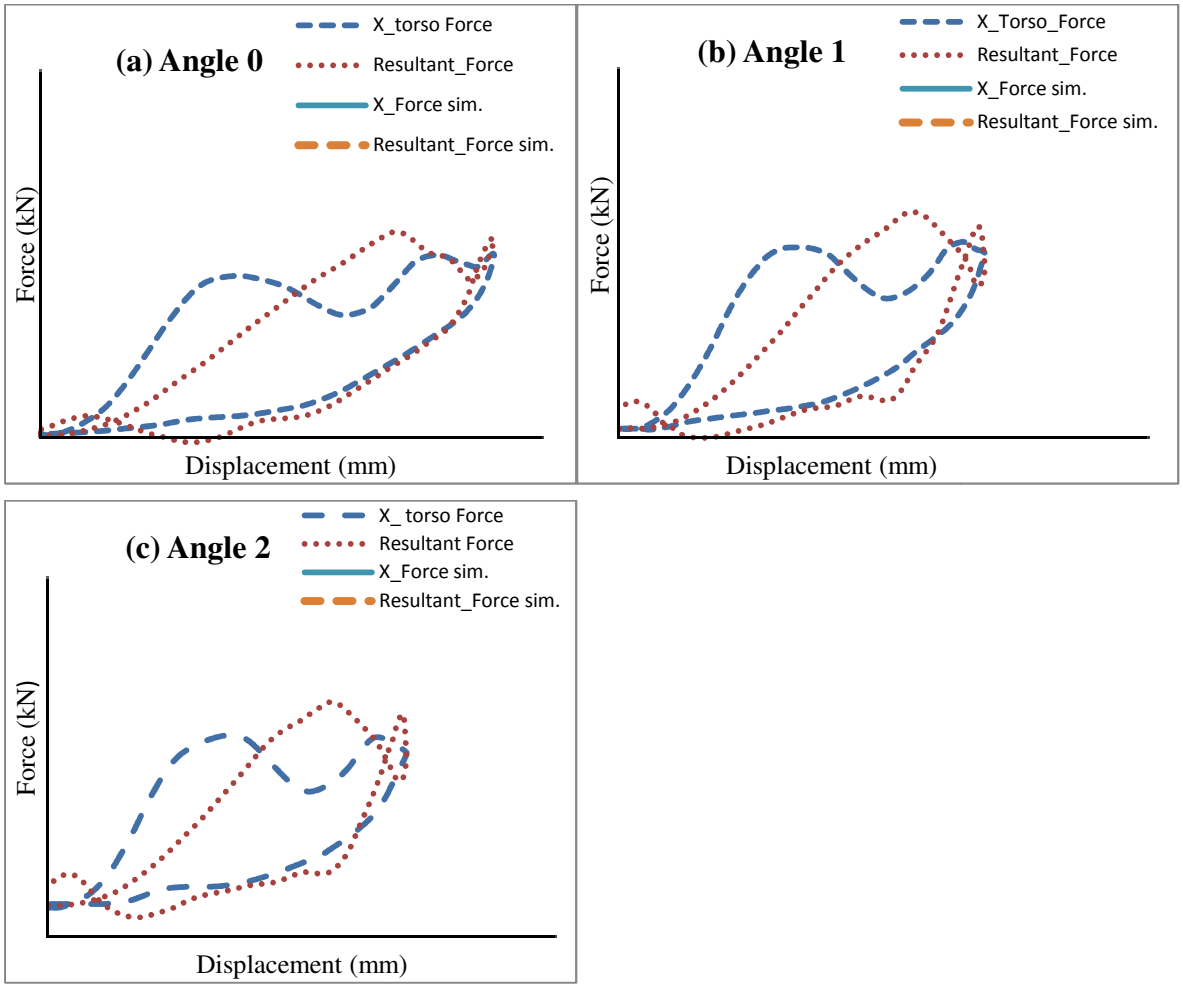

Fig. 3.3 Contact force for the body block

4 Discussion

An impact test setup was identified as the most appropriate setup for the current study, and then replicated both in physical testing and FE modeling. Sensitivity of steering wheel to different tilt angles of the rim was investigated during physical testing. Comparison to the simulation was performed to see the similarities and differences; to validate the FE model. Physical and FE model response changes with the tilt angle of the rim. For 0 and 10 degree tilt angles, the rim sliding was found more significant, both during simulation and testing. This causes the spokes to take most of the loading from impact plate. Results for force level for 0 and 10 degree both from physical tests and simulation, are almost in the same range, whereas they vary for impact plate horizontal displacement. For 20 and 30 degree tilt angles, the rim takes most of the loading from impact plate; hence results in a higher rim deformation on impact. Variation in results for physical tests and simulation is higher than 0 and 10 degree.

Steering wheel position at 0 degree tilt angle causes spokes to take most of the loading from the impact plate. The steering wheel behavior is stiff during testing, in terms of horizontal displacement of the impact plate. Higher displacement during simulation is due to the rim sliding on impact plate that causes bending of the rim and the spokes. Even though the rim also slides during physical tests, but the foam around the steering wheel takes some of the energy from the impact plate. This makes the steering wheel behave stiffer in testing than simulation, and can result in lower impact plate displacement.

A fall in force level is observed for 0 degree after the initial rise for the curves, both from testing and simulation. This fall can be due to sliding of the rim on the impact plate, which results in a decrease in resistance offered by the rim. After this fall in force, a rise is observed again for all the curves. This rise can be due to resistance offered by the rim and spokes after they are bent to their maximum capacity, and can't be bent or deformed any further, so these components start to resist the impact plate again. Force-displacement curve, for simulation and Test 1 also shows that force starts to reduce prior to maximum horizontal displacement of the plate, which is the indicative of the rim sliding that changes the point of loading.

For 10 degree tilt angle, a stiff behavior of the steering wheel is observed in physical tests, same as for 0 degree tilt angle. Due to steering wheel position, besides rim part of loading is also taken up by the rear spokes. Test results and simulations show that the rim and spokes show resistance to the applied force and do not bend initially. This causes initial rise in force level. Higher rim deformation is observed, as it takes most of the energy from plate. However, the rim sliding on the plate is also observed, due to which the rim shows some bending about Y-axis. As a result of the rim deformation and bending, the resistance offered by the components decreases; hence force level drops slightly after the elastic zone. After this drop in force level, a rise in force level is observed, which can be due to deformation hardening of the rim and spokes. For physical tests, force level starts to fall prior to the maximum horizontal displacement of the impact plate same as for the 0 degree tilt angle, which indicates change in loading path and the rim sliding. Horizontal displacement of the impact plate was found to be higher for simulation than physical tests. This can be due to the foam around the rim, which absorbs energy from the impact plate. Moreover this can also reduce the final deformation of the rim.

The absence of foam in FE model is thought to be one of the major reasons of soft behavior, during simulation. For the right comparison of the FE model and the steering wheel, this foam is required to be modeled in FE. This can increase the ability of FE model to absorb more energy from the impact plate, which can restrict the impact plate motion, rim

deformation and may result in a higher force level. But, on the other hand, this will also increase the CPU time for running the simulation, as the reason for the simplified model was to reduce the simulation time.

The rear and the front spokes also take some of the loading from the impact plate during 0 and 10 degree tilt angle positions. A separate component testing must be performed in future, in order to verify the mesh properties, and to notice the behavior of the spokes and the rim under impact loading from different impact directions.

The behavior of steering wheel during 20 and 30 degree tilt angles is nearly similar, both during simulation and physical tests. However, simulation results differ widely from the physical test results. The position of steering wheel at these angles causes the rim to take most of the loading from the impact plate, which results in higher rim deformation. For the physical tests, due to the rim deformation, force level falls after the initial rise. The region around the connection between rear spokes and the rim is found to be highly stress concentrated, as indicated by the fracture of foam in Test 5 and Test 7. The rim deforms until it hits the upper part of the hub. The foam around the steering wheel narrows the gap between the rim and the hub and the plate cannot move any further. Due to deformation hardening of the rim and spokes, they start to resist the impact plate again. As a result, force level rises to the peak value before the rebound. This behavior during physical tests is different from simulation. During simulation for 20 and 30 degree, the rear spokes do not appear to bend to a large extent; as a result the rim also does not show any notable bending similar to physical tests. The rim sliding is also negligible. Hence, the rim observes much higher deformation than 0 and 10 degree. But due to absence of foam in FE model, the gap between hub and the rim is more than the steering wheel. The rim continues to deform, and the impact plate moves further without any significant resistance offered by the rim or spokes. As a result, force level after the initial rise remains steady for 20 degree tilt angle, and continues to fall gradually for 30 degree.

As a future work, to increase the rim thickness can be an alternative to compensate for foam in FE model. This foam due to its thickness appeared to block the impact plate displacement during physical testing for 20 and 30 degree tilt angles. This foam is 10 mm thick, and since deformation of the rim is higher in 20 and 30 degree tilt angles, so it narrows the gap between the rim and hub, and does not allow any further displacement of the impact plate. Steering wheel can also be tested without any foam, under the same loading conditions. This will widen the gap between the rim and the hub, and the rim will have more space for deformation.

In order to raise the force level and to lower the impact plate displacement for FE model during 20 and 30 degree tilt angles, material tuning of the FE model can also be an option. To estimate the Young's modulus, Poisson's ratio and plastic region properties, Universal Tensile Testing (UTT) machine can be used to perform tensile tests of the steering wheel. This will verify the material used for different components of the FE model, and will also provide an estimate of how much these parameters can be varied. As a future work, material testing is recommended using proper test specimens for tensile testing machine.

In general, the current FE model usability is found higher for 0 and 10 degree tilt angles. For a better agreement of physical testing with simulations for 0 and 10 degree load cases, modeling of foam and component testing must be taken in account, which can increase the model usability. However, physical testing results for 20 and 30 degree differ widely from simulations. To reach a better agreement for 20 and 30 degree load cases, several options must be considered in future, such as, increasing the rim thickness, testing the steering wheel without any foam and material tuning.

5 Conclusion

The objective of this study was to validate the already existing FE steering wheel model, and to design and build an appropriate physical test setup. The validity of the model and its usability was concluded using the corridor limits and visual inspection of graphs. The main findings of this thesis study are:

- Physical and FE model response changes with the tilt angle of the rim. During physical testing, highest force level was observed for 20 degree, and highest impact plate displacement was observed for 30 degree tilt angle. While for simulation, highest force level was observed for 10 degree, and highest impact plate displacement was observed for 30 degree tilt angle.

- Fig. 5.1(a) shows the model validity for 0 degree tilt angle using corridor limits. The results are considered valid for the impact plate displacement of 78 mm only. After this limit, the behavior of steering wheel was different both during testing and simulation. The impact plate started to rebound for Test 1 after a rise in force level, and for Test 2, the stopper restricted its motion and resulted a dip in force level. Whereas for simulation, the rim continued its bending, force level increased steadily until the impact plate reached the hub of the steering wheel.

- Results for 10 degree tilt angle are considered valid for 66 mm displacement of the impact plate as shown in Fig 5.1 (b). Beyond this limit, due to higher rim deformation and bending in simulation, force level increased gradually. Whereas, for Test 3, a sharp rise in force level was observed. For Test 4, due to lower energy level, plate already started its rebound.

- Simulation results for 20 and 30 degree were found out of corridor limits as shown by Fig. 5.1 (c) and (d), and hence not considered as validated. Due to presence of foam during physical testing, higher compressive stiffness was seen than simulation. On the other hand, due to absence of foam during simulation, resistance offered to the impact plate was lower and force level could not reach the corridor limits after the elastic zone.

- Higher stiffness of FE steering wheel model is required to have a much better match to the test results. Modeling of the foam can be the other alternative.

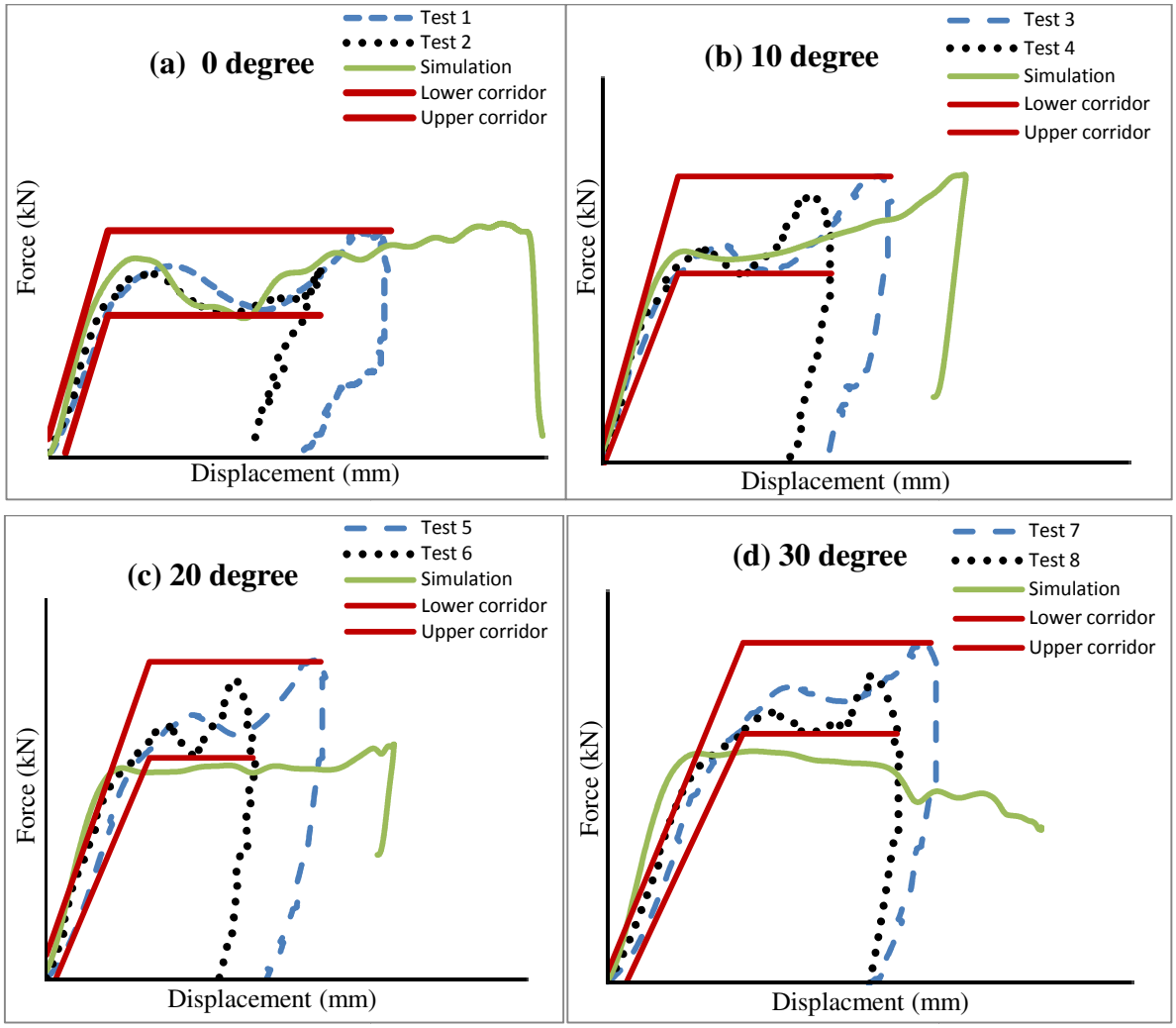

Fig. 5.1 FE model validation using corridor limits. The upper corridor limit was set by taking the maximum force level, and lower corridor limit was set by taking the minimum force level after the elastic zone.

6 References

[1] (2011-05-18) Anders Lundqvist; *Swedish Road Administration., Road safety solutions in Sweden.*

[2] (2011-05-19) Holmqvist, Kristian (2009): *Chest Injuries in Heavy Vehicle Frontal Collisions-Evaluation and Adaptation of the Hybrid III Dummy Instrumentation and Injury Reference Values by Means of Human Body Modeling*. Göteborg: Chalmers University of Technology.

[3] (2011-05-19) Holmqvist, Kristian; Svensson, Mats Y.; Davidsson, Johan; Thorn, Stefan (2009): *Evaluation of Hybrid III Thoracic Injury Criteria in Impacts with a Simulated Truck Steering wheel – Suggestions for Modifications in Instrumentation and Reference Values.* International IRCOBI Conference on the Biomechanics of Impact.

[4] (2011-05-19) Holmqvist, Kristian (2010); Svensson, Mats Y.; Davidsson, Johan; Brolin, Karin; Thorn, Stefan: *Challenges in Steering Wheel Rim to Thorax Impacts Using Finite Element Hybrid III and Human Body Models for Heavy Vehicle Frontal Crash Applications.* International IRCOBI Conference on the Biomechanics of Impact.

[5] Gwehenberger, J., Langwieder, K., Bromann, G., Zipfel, D. (2002) *Injury risk for truck occupants due to serious commercial vehicles accidents~Results of real-world-crash analysis*. 2002, International IRCOBI Conference on the Biomechanics of Impact, Munich, Germany. Resource Nr: 2002-13-0007. International Research Council on Biokinetics of Impacts, Bron, France.

[6] (2011-04-26) Sukegawa, Y., Matsukawa, F., Masuda, N. (2001) *Experimental research on truck driver's safety in frontal collision. International Technical Conference on the Enhanced Safety of Vehicles, Amsterdam, The Netherlands.* Resource Nr: 2001-06-0099. National Highway Traffic Safety Administration, Washington, D.C., USA.

[7] CATIA, Version 5, Latest build NO. 21, Dassault Systemes, February 2010.

[8] Hallquist, J., O. (2007) *LS-DYNA Keyword User's Manual.* Livermore Software Technology Corporation. Livermore, California.

[9] Radioss TM, Version 10, Altair Hyperworks, January 2009.

[10] E/ECE/324 Add.112/Rev.3 E/ECE/TRANS/505 May 30, 1994. *Uniform provisions concerning the approval of vehicles with regard to the protection of the driver against the steering mechanism in the event of impact.*

7 Appendix

Appendix A: Material card

Rim

```
*MAT_PIECEWISE_LINEAR_PLASTICITY_TITLE
Rohrstahl Delmas E235CR1 13x1.6 Shell
$#     mid        ro         e        pr      sigy      etan
fail      tdel
    200002 7.8500E-6 192.00000  0.300000     0.000     0.000
0.000     0.000
$#       c         p      lcss      lcsr        vp
     0.000     0.000   2330147         0 -1.000000
$$ HM Entries in Stress-Strain Curve =         8
$#    eps1      eps2      eps3      eps4      eps5      eps6
eps7      eps8
     0.000     0.000     0.000     0.000     0.000     0.000
0.000     0.000
$#     es1       es2       es3       es4       es5       es6
es7       es8
     0.000       0.000       0.000       0.000       0.000       0.000
0.000     0.000
```

Rear spokes

```
*MAT_PIECEWISE_LINEAR_PLASTICITY_TITLE
Rundstahl Austria S235JRG2C+C - 6 Shell
$#     mid        ro         e        pr      sigy      etan
fail      tdel
    200004 7.8500E-6 196.00000  0.300000     0.000     0.000
0.000     0.000
$#       c         p      lcss      lcsr        vp
     0.000     0.000   2330148         0 -1.000000
$$ HM Entries in Stress-Strain Curve =         8
$#    eps1      eps2      eps3      eps4      eps5      eps6
eps7      eps8
     0.000     0.000     0.000     0.000     0.000     0.000
0.000     0.000
$#     es1       es2       es3       es4       es5       es6
es7       es8
     0.000     0.000     0.000     0.000     0.000     0.000
0.000     0.000
```

Front spokes

```
*MAT_PIECEWISE_LINEAR_PLASTICITY_TITLE
Rundstahl Austria S235JRG2C+C - 8 Shell
$#     mid        ro         e        pr      sigy      etan
fail      tdel
    200005 7.8500E-6 200.00000  0.300000     0.000     0.000
0.000     0.000
$#       c         p      lcss      lcsr        vp
     0.000     0.000   2330149         0 -1.000000
$$ HM Entries in Stress-Strain Curve =         8
$#    eps1      eps2      eps3      eps4      eps5      eps6
eps7      eps8
```

```
     0.000     0.000     0.000     0.000     0.000     0.000
0.000     0.000
$#     es1       es2       es3       es4       es5       es6
es7       es8
     0.000       0.000       0.000       0.000       0.000       0.000
0.000     0.000
```

Hub

```
*MAT_PIECEWISE_LINEAR_PLASTICITY_TITLE
AM60 Solid 23 C
$#     mid        ro         e        pr      sigy      etan
fail      tdel
     29001 1.7400E-6 40.849998  0.309000     0.000     0.000
0.000     0.000
$#       c         p      lcss      lcsr        vp
     0.000     0.000   2320011         0 -1.000000
$$ HM Entries in Stress-Strain Curve =         8
$#    eps1      eps2      eps3      eps4      eps5      eps6
eps7      eps8
     0.000     0.000     0.000     0.000     0.000     0.000
0.000     0.000
$#     es1       es2       es3       es4       es5       es6
es7       es8
     0.000     0.000     0.000     0.000     0.000     0.000
0.000     0.000
```

Connectors

```
*MAT_PIECEWISE_LINEAR_PLASTICITY_TITLE
AM60 Solid 23 C
$#     mid        ro         e        pr      sigy      etan
fail      tdel
    200006 1.7400E-6 40.849998  0.309000     0.000     0.000
0.000     0.000
$#       c         p      lcss      lcsr        vp
     0.000     0.000   2330150         0 -1.000000
$$ HM Entries in Stress-Strain Curve =         8
$#    eps1      eps2      eps3      eps4      eps5      eps6
eps7      eps8
     0.000     0.000     0.000     0.000     0.000     0.000
0.000     0.000
$#     es1       es2       es3       es4       es5       es6
es7       es8
     0.000     0.000     0.000     0.000     0.000     0.000
0.000     0.000
```

Body Block

```
*MAT_SIMPLIFIED_JOHNSON_COOK_TITLE
Body_block_Mat
$#     mid        ro         e        pr        vp
    200000 7.8000E-6 207.00000  0.300000     0.000
$#       a         b         n         c    psfail    sigmax
sigsat      epso
  0.458640  0.210000  0.600000  0.049500     0.000
0.5200001.0000E+28 4.8300E-5
```